SAND2015-6592C

Materials compatibility in Dish-Stirling Solar Generators using Cu-Si-Mg eutectic for latent heat storage

A. M. Kruizenga [1, a)] and E.A. Withey[1], C.E. Andraka[2], P.J. Gibbs[1]

[1]*Sandia National Laboratories, P.O. Box 0969, Livermore, CA 94550,*
[2]*Sandia National Laboratories, P.O. Box 5800, Albuquerque, NM 87185*

[a)]amkruiz@sandia.gov

Abstract. Dish-Stirling systems are a strong candidate to meet cost production goals for solar thermal power production. Use of a copper-silicon-magnesium phase change material was investigated as an option for thermal energy storage. This work investigates the ability of commercially available plasma spray coatings, while investigating mechanistic insights into materials for this system. Computed tomography was leveraged as a rapid screening tool to assess the presence of localized attack in tested coatings.

INTRODUCTION

Dish-Stirling systems have been identified as having a strong potential of meeting SunShot cost goals of 6¢/kWh. These systems feature high temperature (700-800 °C), high optical efficiency, high power cycle efficiency, and modularity. We are investigating Cu-Si-Mg eutectic alloy, a metallic phase change material (PCM), for latent heat storage for increased capacity factor and consistent power delivery. The metallic alloy PCM is favored because of its high thermal conductivity, high heat of melting, and melting temperature match to the engine operating range.

This paper identifies the materials compatibility challenges and process made to date in fabricating and containing PCMs for Dish-Stirling systems.

BACKGROUND:

Figure 1 illustrates the proposed integration of energy storage with Dish-Stirling. Heat storage integration results in several key differences from current systems. The Stirling engine would be moved to the back of the dish to be collocated with the PCM storage, rather than having the engine in the dish focus. Placement of both the storage and engine at the rear optimizes the balance of the system, reduces cantilevered weight, and leads to efficient structural designs. The heat pipe design utilizes sodium as the heat transfer medium, where the heat pipe itself is built out of alloy Haynes 230.

PCM chosen is a Cu-Si-Mg alloy, nominally Cu-21.2wt%Mg-25.3wt%Si, with the composition obtained from the ASM Phase Diagram Database[1]. There is some debate within existing literature and computational calculations as to the specific composition of the eutectics within the ternary system [1-5]. Data determined from differential scanning calorimetry (DSC) indicated that the ASM composition had the most repeatable melt and heat flow curves with full melting complete under 800°C.

Containment of the PCM was found to be difficult given the reactivity of magnesium and silicon. Magnesium alloys are typically cast within steel vessels, due to the lack of reaction between magnesium and iron [6]. Liquid silicon has been contained in several materials: SiC, Al_2O_3, Si_3N_4, SiO_2, graphite, and yittria stabilized zirconia [7].

The design choice to have Haynes 230 used for the heat pipes were based upon the relative maturity of liquid sodium compatibility and heat pipe fabrication techniques. The protective interface between the Haynes 230 and the PCM would then require development of a protective coating that could be applied prior to operation. Due to the complex geometry, relatively large size of the system, and compressed development time it was decided to utilize off-the-shelf materials that can be applied via plasma spray or thermal spray technique to allow for a wide range of ceramics. Applications of SiC and Si_3N_4 via plasma spray are currently under development and were subsequently ruled out for this reason [8]. Thus Al_2O_3, SiO_2, carbon, and yittria stabilized zirconia (YSZ) were considered for this application.

Thermodynamic properties of each potential coating and phase change material were evaluated on an oxygen basis and presented in the Ellingham Diagram in Fig. 2.As shown, yittria (Y_2O_3) is most thermodynamically stable, followed by magnesia (MgO) and spinel ($MgAl_2O_4$). Silica (SiO_2) and mullite ($3Al_2O_3$*$2SiO_2$), both relatively common ceramics, are relatively unstable in this system by contrast to other oxides. Silica has been reduced by a magnesiothermic reduction process, which has been observed elsewhere [9], according to the following equation:

$$SiO_2(s) + 2Mg(g) \rightarrow Si(s) + 2MgO(s \quad (1)$$

During fabrication of the PCM it was found to be difficult to retain magnesium in solution at high temperatures (near 1000°C) due to the magnesium's volatility. Experiments were performed and determined that Mg volatility resulted Equation 1 to proceed and was verified using X-Ray Diffraction (XRD). On the basis of reactivity with magnesium, silica was also ruled out as a coating and also provided confidence in the thermodynamic data.

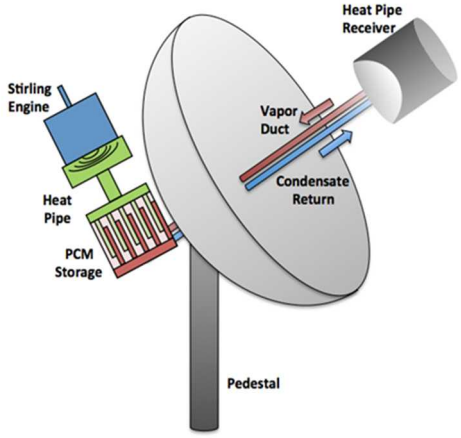

FIGURE 1: Conceptual design of PCM storage on Dish-Stirling system[10].

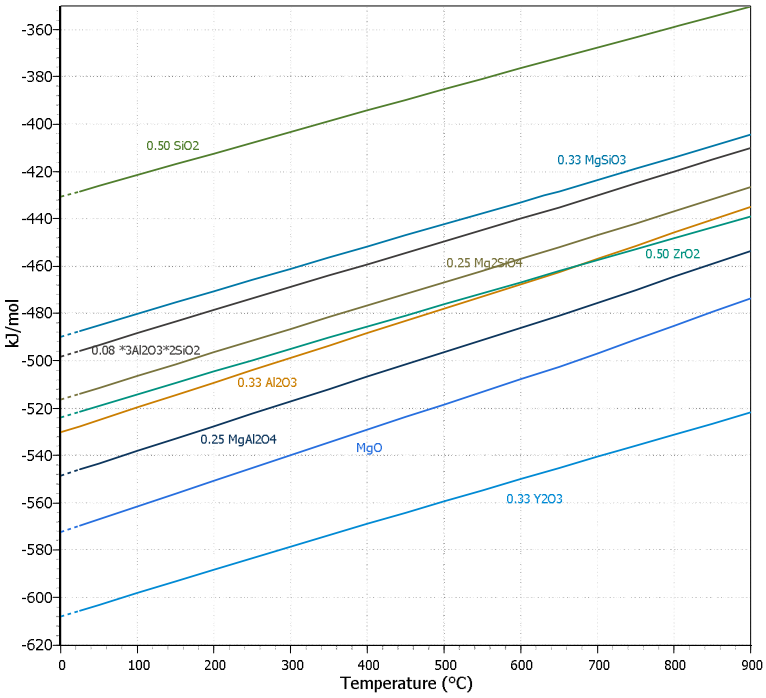

FIGURE 2: Ellingham diagram for selected oxides in Cu-Si-Mg-Al systems [11]

TESTS METHODOLOGY:

PCM heats were obtained in small heats (~50g) from Ames laboratory and were discussed previously [10] of Cu-21.2Mg-25.3Si. For this test series a larger heat was obtained, roughly 2.5kg, of same nominal composition. Unfortunately, due to the larger size, it was found that the alloy was not well mixed and exhibited in some cases non-uniform melting. Ultimately, in order to address this risk of incomplete melting, two test temperatures were utilized, 820°C and 950°C. Based upon the DSC data, this high temperature would result in melting of the PCM regardless of in homogeneities in the melt.

Samples were made from Haynes 230 pipe with ends welded in place, with nominal dimensions of 25mm long, 25mm wide, 12mm deep, and a wall thickness of 1.5mm. Samples were then cleaned and prepped for plasma spray coatings.

Coatings were applied by two vendors: Thermal Spray Technologies (TST) (Sun Prairie, WI) and Falmer Thermal Spray (Salem MA). All samples exposed at 820°C were prepared by TST, while samples used in the 950°C exposure were prepared by Falmer. Regardless of the vendor, each coating consisted of three layers: inner metallic, middle metal/ceramic, and outer ceramic layer. The inner base coat layer was a Ni-20Cr to provide a coefficient of thermal expansion (CTE) match resembling that of Haynes 230. Upon finishing the metallic layer, a roughly 50/50 mixture of Ni-20Cr and ceramic (Al_2O_3, Y_2O_3, YSZ, $MgAl_2O_4$) was applied, which was followed by the final ceramic layer. Total coating thicknesses ranged from 250-350µm.

Sample boats were loaded with approximately 3g of PCM and placed into individual quartz ampules (Fig. 3). Separate ampules were chosen to avoid any convolution of results due to the possibility of volatile produces that may arise during tests. Ampules were evacuated to 10-6 Torr, backfilled to 200 Torr, and then sealed prior to tests. Leaking ampules are detected by a visually transparent clear ampule.

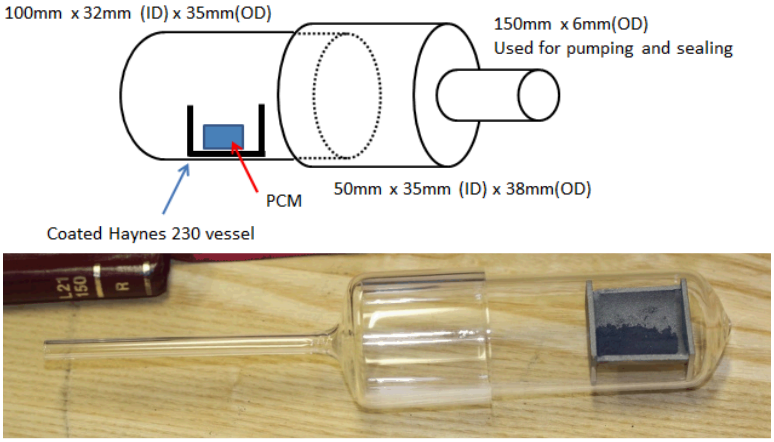

FIGURE 3: Samples were sealed in a quartz vial, pumped down, and back filled with argon.

Samples are placed into a box furnace and heated to temperature over the course of several hours to avoid undue thermal stress on the quartz ampule. Upon reaching temperature samples are held isothermally until the end of the exposure period and then ramped down.

After exposure to PCM, the coated boats were potted in an Argon atmosphere, cross-sectioned, and polished for optical microscopy. Promising results were subject to further analysis using electron microscopy and wavelength dispersive spectroscopy (WDS) using an electron microprobe analyzer (EMPA). It should be noted that the WDS elemental maps obtained from EMPA were are for qualitative purposes and their color scales are not quantitative. These maps can only be used to judge relative amounts of one element as it is distributed across the area in question not to determine the relative quantities of these elements relative to others.

RESULTS AND DISCUSSION:

After 500 hours at 820°C, YSZ had observed coating failures as shown in Fig.4A. The origin of the failure is likely due to chemical incompatibility (versus a point defect or holiday) as there were several locations where coating damage occurred (Fig.4B, Fig.4C). Y_2O_3 was found to have one clear failure (Fig.4E, Fig.4H), with an indication of an artifact in Fig.4F that another failure is developing. No failures were observed on the Al_2O_3 coating (Fig.4I-O) even after cross sectioning several sample locations.

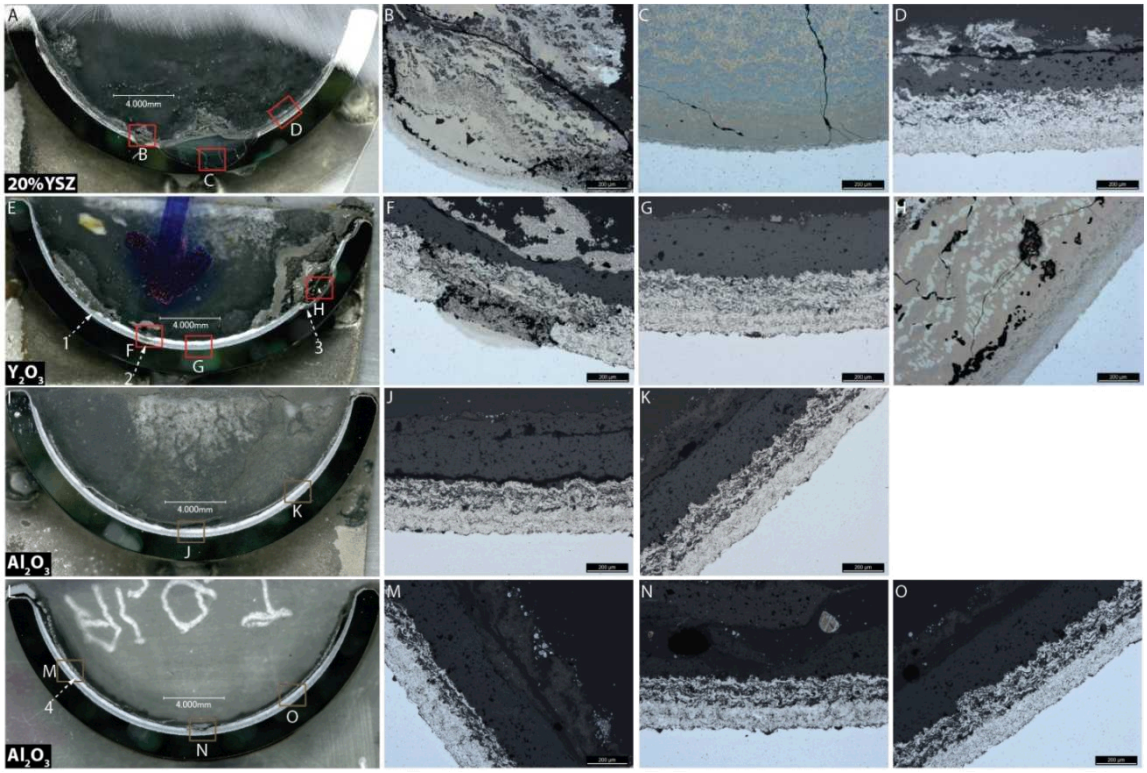

FIGURE 4: Optical microscopy results for the 820°C, 500 hour exposure of (A-D) 20%YSZ, (E-H) Y_2O_3, and (I-O) Al_2O_3 TST coatings.

In order to determine the nature of the Y_2O_3 failure, i.e. flaw versus chemical incompatibility, the coating was analyzed further in the electron microprobe (EMPA) to elucidate where each element of the PCM, coating, and bond layer were at each area of attack. At area 1 in Fig.4E, the Y_2O_3 coating has been almost completely replaced by the PCM (dark mass) although, the intermediate and subsequent layers are still intact. Below the mass of PCM there is a small stained area in what remains of the coating-intermediate layer interface. In this area, the Mg map in Fig.5 illustrates that Mg has infiltrated the coating and is working its way through the intermediate layer, while Cu and Si remain trapped in the PCM and outer areas of the remaining Y_2O_3 coating. EMPA results for area 2 from Fig.4E are shown in Fig.6.

Optically, this area appears to have been attacked slightly more than Area 1 with a larger darker stain. Figure 6 shows that Mg has further infiltrated the intermediate layer where Si is densely distributed. Copper has sparsely entered this area. It should also be noted that the oxygen density is larger in the stained area than outside of it. Finally in Area 3, the coating was completely consumed by PCM and the Haynes 230 fully attacked, as evidenced by the presence of several diffusion layers visible in Fig.4E and H. Figure 6 indicates that attack of Haynes 230 is dominated by Si and not Mg. This is expected as silicon is known to be highly reactive, has a reasonable solubility in both Ni and Cr, and can form multiple Cr-Ni silicides at the testing temperature. We believe that the initial degradation of the coating, leading to eventual attack of the Haynes 230, occurs through a reaction between the Y_2O_3 and Mg via Equation 2:

$$Y_2O_3 + 3Mg \leftrightarrow 2Y + MgO \quad (2)$$

Because the Gibbs energies of both Y_2O_3 and MgO are similar at the test temperature, it is likely that an equilibrium amount of MgO 1 reducing the Y_2O_3 to yttrium. In doing this, there is volume change which would create a pathway for Si penetrate the coating, intermediate, and bond layers to attack the Haynes 230.

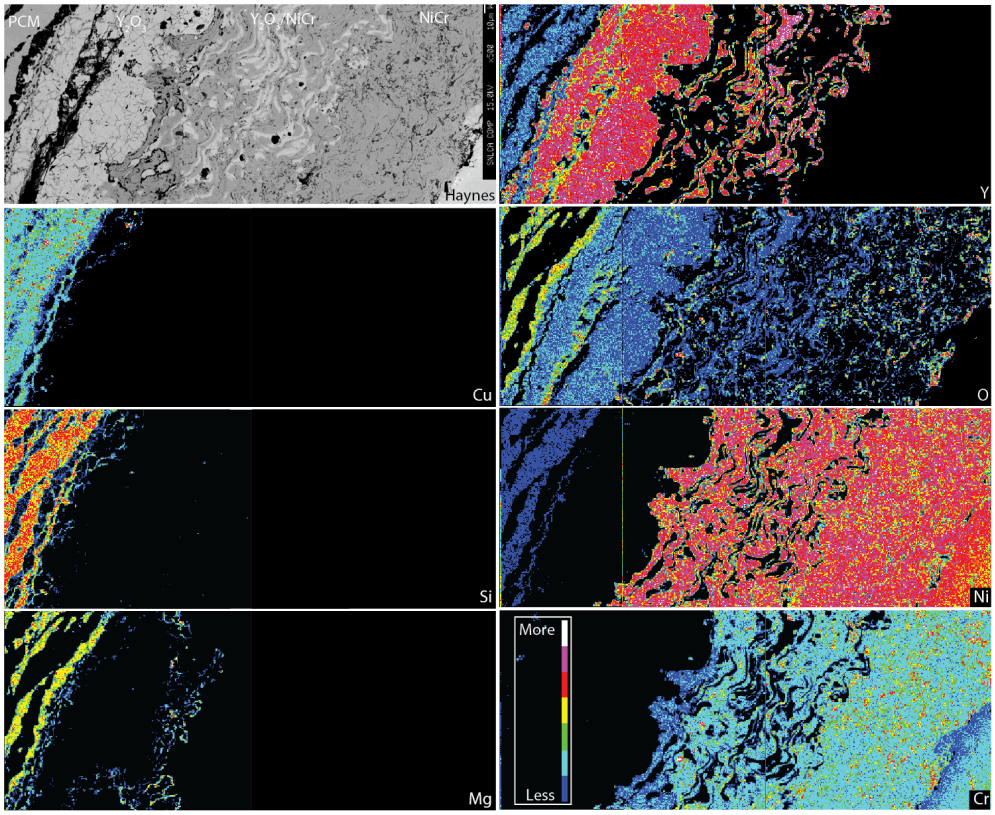

FIGURE 5: Electron microprobe analyzed from area 1 on Fig.4E showing initial infiltration of Y_2O_3 coating with magnesium.

Similar analysis was performed on the Al_2O_3 and determined magnesium infiltrated the Al_2O_3 coating. The overlap of intensity of Mg, Al, and O in Fig.7 is indication of preferential interaction between Mg and the Al_2O_3 coating, likely by the formation of $MgAl_2O_4$ spinel. This compound is usually produced from MgO and Al_2O_3. Based on thermodynamics, Mg first reduced Al_2O_3 to form MgO, and then reacted with the remaining Al_2O_3 to form $MgAl_2O_4$ via Equation 3 and 4:

$$Al_2O_3 + 3Mg \leftrightarrow 2Al + 3MgO \quad (3)$$

$$Al_2O_3 + 3MgO \leftrightarrow MgAl_2O_4 \quad (4)$$

This reaction would cause volumetric changes that may result in cracking or a lack of mechanical adhesion. Given the likely evolution of $MgAl_2O_4$ during exposure this material was included in the next series of testing.

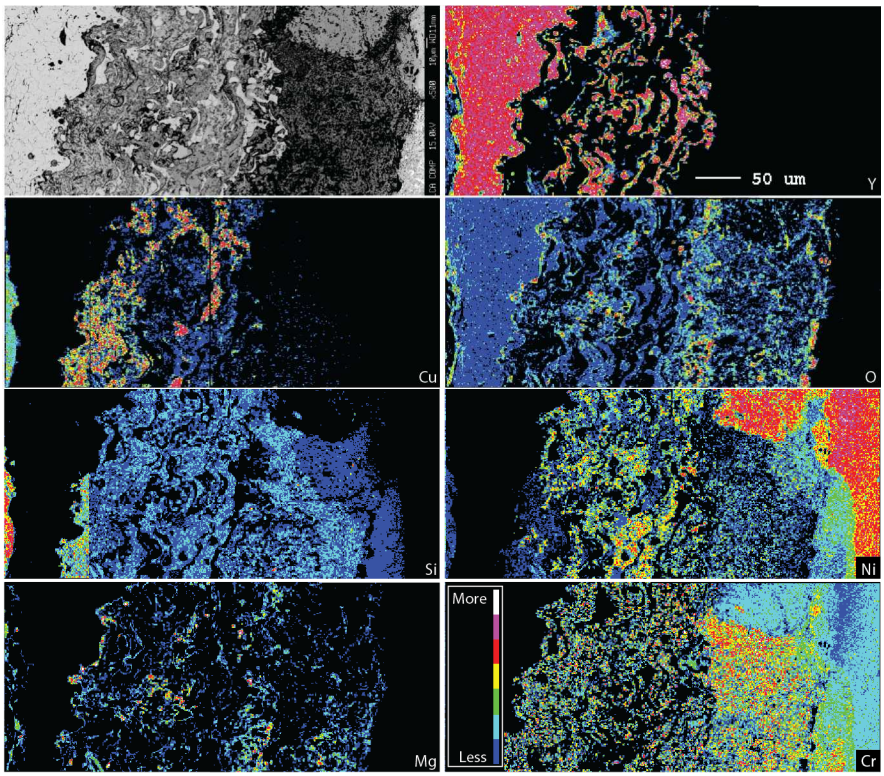

FIGURE 6: Electron microprobe analyzed Area 2 from Fig.4E showing subsequent infiltration of Y_2O_3 coating with silicon after Mg.

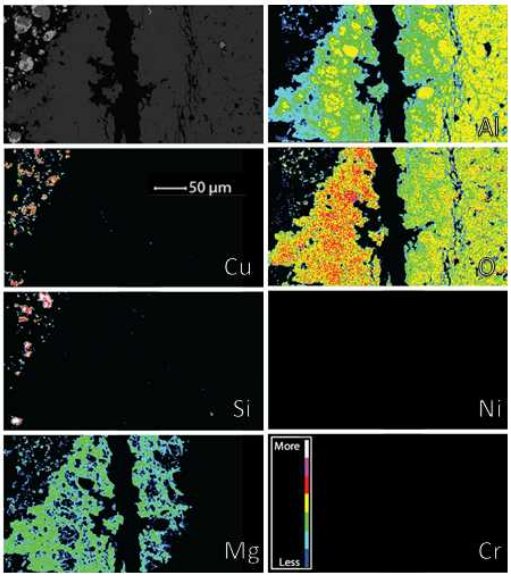

FIGURE 7: EMPA results for the Area 4 in Fig. 4L showing the interaction of Mg with Al_2O_3 coating. PCM interface is on the far left of the image.

Test 2 samples were prepared by Falmer and were exposed for 500 hours at 950°C where Al_2O_3 and $MgAl_2O_4$ were investigated. In order to scan the entire sample for possible failures micro computed tomography (CT) was utilized to look for defects or failures in the coating. Figure 8 has representative CT images of Al_2O_3 and $MgAl_2O_4$,

where clear coating defects are observed in discrete locations of the alumina. Microscopy was used to identify the reason behind these obvious defects or failures on the Al_2O_3 coatings.

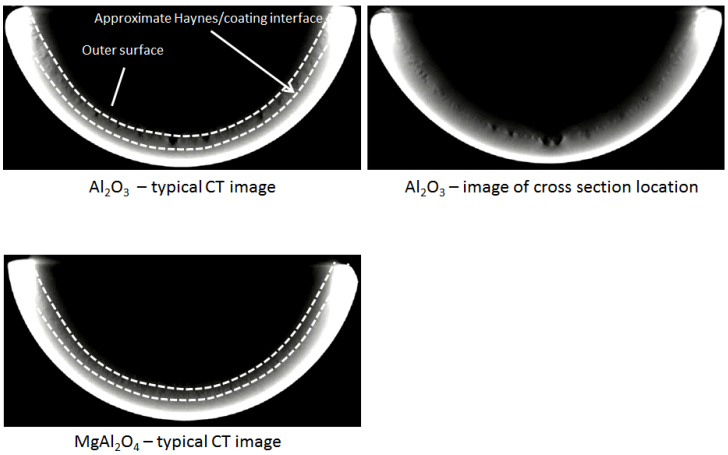

FIGURE 8: CT images of both materials post exposure, showing both typical images and locations of cross for microscopy.

Energy dispersive spectroscopy was used to generate x-ray maps, as shown in Fig.9, of the Al_2O_3 coating in locations where no failures were observed. Al_2O_3 layers were found to be relatively thin, roughly 40µm. By comparison, the metallic/ceramic transition layer is five times thicker (~240 µm) and the metallic layer is three times thicker (~140 µm). Thus the observed failure may be a result of the thin coating layer.

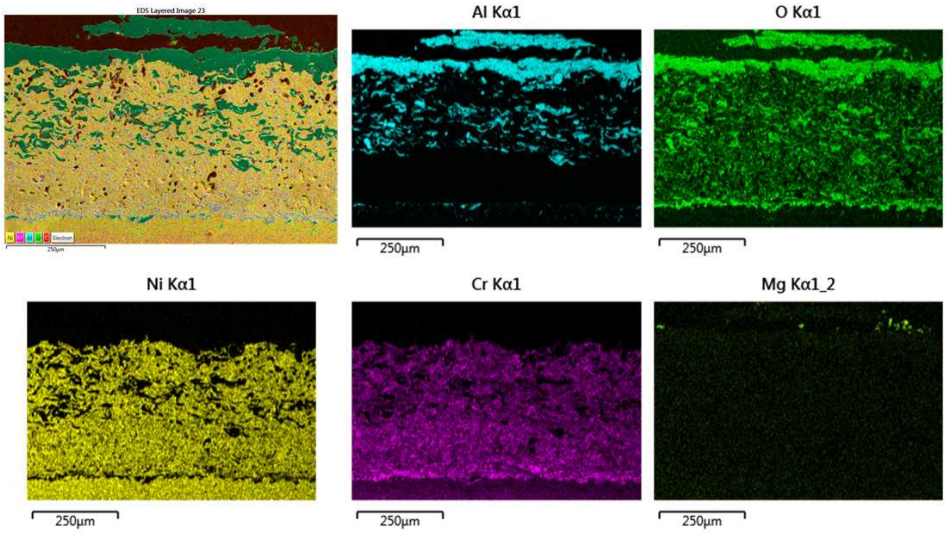

FIGURE 9: EDS map of intact alumina. Top, left image is an elemental composite. Alumina is the outer layer, with a transition layer of NiCr, followed by a pure bottom layer of NiCr.

One failure location was investigated (Fig. 10) and from this two observations are noted. First, as expected, regions of metallic nickel tend to interact with the copper and silicon from the PCM. Figure 11B indicates that the intrusion of PCM is currently limited to the metallic/ceramic transition layer, where the magnesium elementally leads the attack. This would suggest that there is not a mechanistic change from lower temperature tests, but only a kinetics increase.

(a)

(b)

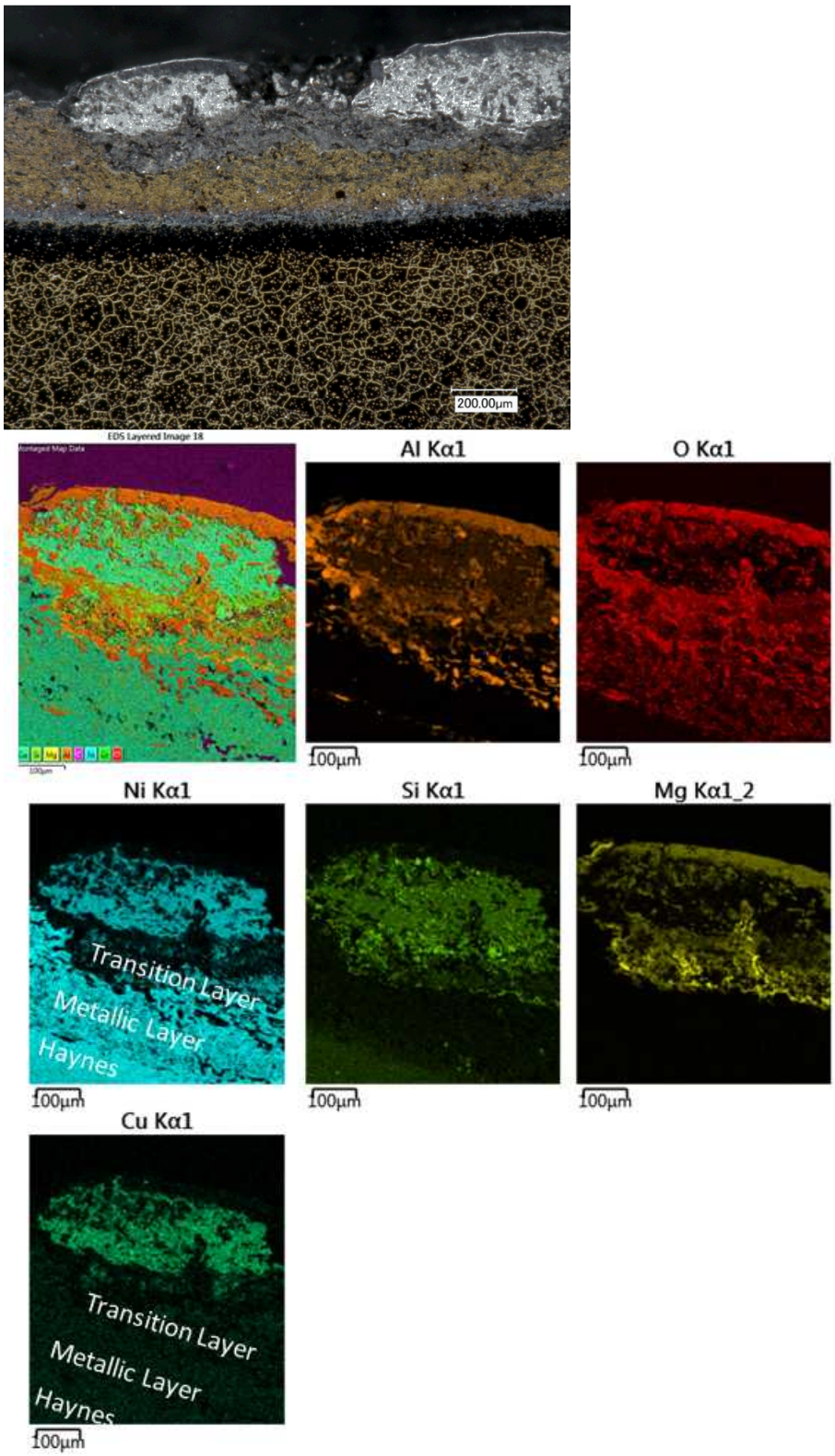

FIGURE 10: a) Optical image of apparent coating attack. b) EDS image of attacked region. Mg, Al, and O are highly correlated, while Si, Cu, and Ni are correlated in the coating region.

CONCLUSIONS

Yittria as a coating had failures despite the relative thermodynamic stability by comparison to other possible oxide formed in this system. This failure is thought due to the volumetric change between equilibrium concentrations of magnesia and yittria, which resulted in mechanical degradation of the coating. Alumia performed without apparent issue at the 820°C for 500 hours. Magnesium enrichment of the alumia layer was observed through the formation of magnesium aluminum spinel.

While alumina did work for short duration experiments at 820°C, when raising the temperature to 950°C the kinetics appeared to increase by localized failures of the alumina layer and infiltration of the phase change material into the transition layer. Interaction of the nickel with silicon and copper was observed and, as with the low temperature experiments, magnesium enrichment preceded other phase change elements. Use of $MgAl_2O_4$ was suggested due to the natural formation of this oxide and preliminary experiments are encouraging in the use of this plasma spray coating.

Computed Tomography was utilized in locating possible defects/failures that may occur during operation. This technique was extremely useful in both focusing microscopy efforts, while scanning the entire length of samples. Scan of the entire sample would not be possible from a microscopic standpoint. This technique will be used in future exposures to reduce the amount of microscopy performed and assess larger areas not yet possible with microscopy.

ACKNOWLEDGEMENTS

Sandia National Laboratories is a multi-program laboratory managed and operated by Sandia Corporation, a wholly owned subsidiary of Lockheed Martin Corporation, for the U.S. Department of Energy's National Nuclear Security Administration under contract DE-AC04-94AL85000, SANDXXXX-XX

REFERENCES

1. ASM International, (2012).
2. D. Farkas and C. E. Birchenall, Metall and Mat Trans A **16** (3), 323-328 (1985).
3. a. G. T. CRCT- Thermfact Inc., (2010).
4. C. E. Birchenall, S. United, E. Department of, S. Division of Energy Storage, C. Lewis Research, D. University of and E. Department of Chemical, *Heat storage in alloy transformations : final report*. (The Division ; For sale by the National Technical Information Service, Washington, D.C.; Springfield, Va., 1981).
5. C. E. Birchenall and A. F. Riechman, MTA Metallurgical Transactions A **11** (8), 1415-1420 (1980).
6. A. A. Luo, Journal of Magnesium and Alloys **1** (1), 2-22 (2013).
7. Y. Sato, Y. Kameda, T. Nagasawa, T. Sakamoto, S. Moriguchi, T. Yamamura and Y. Waseda, Journal of Crystal Growth **249** (3–4), 404-415 (2003).
8. Z. Károly, C. Bartha, I. Mohai, C. Balázsi, I. E. Sajó and J. Szépvölgyi, International Journal of Applied Ceramic Technology **10** (1), 72-78 (2013).
9. Z. Bao, M. R. Weatherspoon, S. Shian, Y. Cai, P. D. Graham, S. M. Allan, G. Ahmad, M. B. Dickerson, B. C. Church, Z. Kang, H. W. Abernathy Iii, C. J. Summers, M. Liu and K. H. Sandhage, Nature **446** (7132), 172-175 (2007).
10. C. E. Andraka, A. M. Kruizenga, B. A. Hernandez-Sanchez and E. N. Coker, Energy Procedia **69**, 726-736 (2015).
11. Outotec, (2013).